PROCEEDINGS OF SPIE

SPIEDigitalLibrary.org/conference-proceedings-of-spie

Diffuse tomography of optical anisotropy of tumors of the uterus wall

A. G. Ushenko, V. G. Zhytaryuk, M. I. Sidor, O. Ya. Wulchulyak, A. V. Motrich, et al.

A. G. Ushenko, V. G. Zhytaryuk, M. I. Sidor, O. Ya. Wulchulyak, A. V. Motrich, I. V. Soltys, O. V. Pavliukovich, N. Pavliukovich, "Diffuse tomography of optical anisotropy of tumors of the uterus wall," Proc. SPIE 10728, Biosensing and Nanomedicine XI, 107280Q (5 September 2018); doi: 10.1117/12.2320529

SPIE.

Event: SPIE Nanoscience + Engineering, 2018, San Diego, California, United States

Diffuse tomography of optical anisotropy of tumors and necrotic conditions of biological tissues

A.G. Ushenko[1*], V.G. Zhytaryuk[1], M.I.Sidor[1], O. Ya. Wanchulyak[2], A.V. Motrich[1], I.V. Soltys[1], O.V.Pavliukovich[2], N.Pavliukovich[2]
[1]Chernivtsi National University, 2 Kotsiubynskyi Str., Chernivtsi, Ukraine, 58012
[2] Bukovinian State Medical University, 3 Theatral Sq., Chernivtsi, Ukraine, 58000

o.ushenko@chnu.edu.ua

ABSTRACT

An optical-physical system for extracting information about the fluctuations in the optical anisotropy of strongly scattering biological tissues is considered. A model is proposed for the formation of a depolarized background by birefringent and dichroic structures. An explicit form and symmetry of the completely depolarized component of the Mueller matrix is determined, a second-order differential matrix. An algorithm for the analytic determination of the distributions of elements of a second-order differential matrix is found. Interrelations between the magnitude of the elements of the second-order differential matrix and the fluctuations of the linear and circular birefringence-dichroism are obtained. The technique of diffuse tomography of an optically anisotropic component of strongly scattering biological tissues has been developed and experimentally tested. Maps of the distributions of the elements of the completely depolarized component of the Mueller matrix of the histological sections of the internal organs of the healthy and of the diabetic rats . The sensitivity, specificity and balanced accuracy of the method of diffuse tomography of the polycrystalline structure of tumors of the uterine wall and the degree of hemorrhage of the liver are determined.

Keywords: tomography, anisotropy, biologigal tissue, diagnostics.

1. Theoretical bases that is exceptual to aprobacy to the method of diffusive tomography of the biological tissue

1.1. Introduction

Most biological tissues have an optically anisotropic structure [1-8]. In turn, such a polycrystalline component is closely related to the morphological structure and physiological state of the human organs [9-14]. Therefore, research of such interconnections is an actual task. One of the most informative methods of this diagnosis is Muller-matrix polarimetry [15-19]. This method carries important information on polarization manifestations of optical anisotropy of biological layers [20-25]. However, most real biological objects scatter light very much. As a result, the uniqueness of the relationship between the distribution of elements of the Müller matrix and the parameters of birefringence and dichroism of the polycrystalline component of biological tissues is lost [25-27]. Our work is aimed at generalizing and expanding the functionality of Muller-matrix polarimetry in the case of differential diagnosis of changes in optical anisotropy of diffuse biological tissues of the uterus wall (oncology) and of the liver (different degrees of blood loss).

1.2. Differential matrix of the 2nd order

In [28-33] a model of the differential expansion of the Müller matrix of multilayered biological tissues in the form of antisymmetric (polarized) and symmetric (depolarized) components was developed.
It is shown that the symmetric or diffuse component ($\{\tilde{N}\}$) of the Müller matrix (φ_{ik}) is determined by the following operator

Biosensing and Nanomedicine XI, edited by Hooman Mohseni, Massoud H. Agahi, Manijeh Razeghi, Proc. of SPIE Vol. 10728, 107280Q · © 2018 SPIE
CCC code: 0277-786X/18/$18 · doi: 10.1117/12.2320529

$$\left\{\widetilde{N}\right\}=0{,}5r^{-2}\left\|\begin{array}{cccc}\ln\varphi_{11} & \ln\left(\frac{\varphi_{12}}{\varphi_{21}}\right) & \ln\left(\frac{\varphi_{13}}{\varphi_{31}}\right) & \ln\left(\frac{\varphi_{14}}{\varphi_{41}}\right)\\ \ln\left(\frac{\varphi_{21}}{\varphi_{12}}\right) & \ln\varphi_{22} & \ln\left(\varphi_{23}\varphi_{32}\right) & \ln\left(\varphi_{24}\varphi_{42}\right)\\ \ln\left(\frac{\varphi_{31}}{\varphi_{13}}\right) & \ln\left(\varphi_{32}\varphi_{23}\right) & \ln\varphi_{33} & \ln\left(\varphi_{34}\varphi_{43}\right)\\ \ln\left(\frac{\varphi_{41}}{\varphi_{14}}\right) & \ln\left(\varphi_{42}\varphi_{24}\right) & \ln\left(\varphi_{43}\varphi_{34}\right) & \ln\varphi_{44}\end{array}\right\|. \quad (1)$$

1.3. Algorithms for evaluating the polycrystalline structure of diffuse biological layers

For strongly depolarizing (diffuse) biological layers, the magnitude of the degree of depolarization as a superposition of non-zero values of the diagonal elements of the Müller matrix is used as the main diagnostic parameter $\varphi_{ii} \neq 0$

$$\Lambda = 1 - \frac{1}{3}\left\{\varphi_{22} + \varphi_{33} + \varphi_{44}\right\}. \quad (2)$$

In our work, the Müller-matrix algorithms for diffusion tomography are reproduction of distribution distributions of the variance of the fluctuations of the parameters of linear and circular birefringence and the dichroism of an optically thick biological layer.

To this end, the "two-wave" approach [15,16,34-37] was established to differentiate the manifestations of birefringence and dichroism of optically anisotropic biological layers. Consider two cases. The first one, when the mechanisms of optical anisotropic absorption can be neglected. Such a situation can be experimentally implemented by appropriate selection of wavelength, probing biological layer, laser radiation. It is known that the spectral absorption maxima of most protein molecules of biological tissues and amino acids of biological fluids fall on the ultraviolet region. Therefore, experimentally such conditions are realized in the "red - λ_1" section of the spectral range.

Using this assumption, it can be shown that the dispersion of the fluctuations of the circular ($D_\varphi(\lambda_1)$) and linear ($D_\delta(\lambda_1)$) birefringence of the polycrystalline component of the biological layer is determined by the following expressions

$$D_\varphi(\lambda_1) = \frac{1}{r^2}\ln\left(\varphi_{44}(\lambda_1)\cdot\left(\varphi_{22}(\lambda_1) + \varphi_{33}(\lambda_1)\right)^{-1}\right); \quad (3)$$

$$D_\delta(\lambda_1) = \frac{1}{r^2}\ln\left(\left(\varphi_{44}(\lambda_1)\right)^{-1}\right), \quad (4)$$

In the short-wave, "blue" (λ_2) section of the spectrum of irradiation of histological sections of biological preparations, the expressions for the variance of the parameters of phase and amplitude anisotropy acquire the following form

$$D_\varphi(\lambda_2) = \frac{\lambda_1}{\lambda_2}\frac{1}{r^2}\ln\left(\varphi_{44}(\lambda_2)\cdot\left(\varphi_{22}(\lambda_1) + \varphi_{33}(\lambda_2)\right)^{-1}\right); \quad (5)$$

$$D_\delta(\lambda_2) = \frac{\lambda_1}{\lambda_2}\frac{1}{r^2}\ln\left(\varphi_{44}(\lambda_2)\right)^{-1}; \quad (6)$$

$$D_\tau(\lambda_2) = \frac{1}{r^2}\left(\ln\left(\varphi_{44}(\lambda_2)\right)^{-1} - \frac{\lambda_1}{\lambda_2}\ln\left(\varphi_{44}(\lambda_1)\right)^{-1}\right); \quad (7)$$

$$D_{\chi} = \frac{1}{r^2}\left(2\ln\left(\varphi_{22}(\lambda_2)\right)^{-1} - \ln\left(\varphi_{44}(\lambda_2)\right)^{-1} - \ln\left(\varphi_{44}(\lambda_1)\right)^{-1}\right). \quad (8)$$

Thus, in the framework of the differential Müller-matrix approach to mapping an optically anisotropic polycrystalline structure of biological layers, we obtained a set of algorithms (relations (3) - (8)) of reproduction of the magnitudes of fluctuations of the parameters of linear and circular birefringence ($D_{\delta}(\lambda_1), D_{\varphi}(\lambda_1)$) and dichroism ($D_{\tau}(\lambda_2)$, $D_{\chi}(\lambda_2)$).

In the future, coordinate distributions $\begin{Bmatrix} D_{\delta}(x,y,\lambda_1) \\ D_{\varphi}(x,y,\lambda_1) \\ D_{\tau}(x,y,\lambda_2) \\ D_{\chi}(x,y,\lambda_2) \end{Bmatrix}$ will be called diffusion tomograms DT.

1.4. Maps of fluctuations of circular birefringence and dichroism of histological slices of the kidneys of the healthy and of the diabetic rats

The method of experimental measurement of the coordinate distributions of the size of elements of the Müller matrix of histological sections of biological tissues is given in detail in [15-17] in fig. 1 and fig.2. The results of the diffusion tomography method (relations (1) - (8)) are two-dimensional maps $L_j(x,y)$ and histograms $N(D_j)$ of the distribution of the magnitude of the fluctuations of circular birefringence D_{θ} (Fig. 1) and dichroism D_{χ} (Figure 2) of the polycrystalline structure of the optic-thick ($\tau = 1{,}19 - 1{,}23; \Lambda = 73\% - 76\%$) histological sections of the tissues of the kidney healthy (fig. 1, fig. 2, fragments (1), (2)) and of the diabetic (fig. 1, fig. 2, fragments (3), (4)) rats.

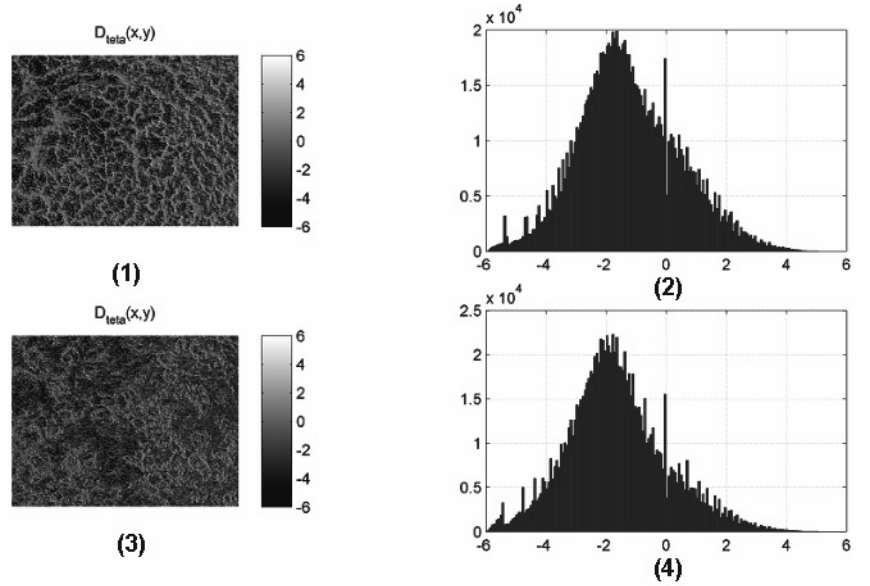

Fig. 1. The maps (fragments (1), (3)) and distribution histograms (fragments (2), (4)) of the magnitudes of circular birefringence fluctuations of the optically thick ($\tau = 1{,}19 - 1{,}23; \Lambda = 73\% - 76\%$) histological sections of the kidney are healthy (fragments (1), (2)) and of the diabetic (fragments (3), (4)) rats.

Comparative analysis of diffusion tomograms $D_{\theta,\chi}(x,y)$ (fragments (1), (3)) and histograms of distributions $N(D_{\theta,\chi})$ (fragments (2), (4)) of the magnitude of the fluctuations of circular birefringence (Fig. 1) and dichroism (Fig. 2) of optically thick ($\tau = 1{,}19 - 1{,}23; \Lambda = 73\% - 76\%$) histological sections Kidneys healthy (fragments (1), (2)) and of the diabetic rats (fragments (3), (4)) showed an increase in the mean and spread range of values of such parameters in maps $D_{\theta,\chi}(x,y)$ of pathologically altered specimens.

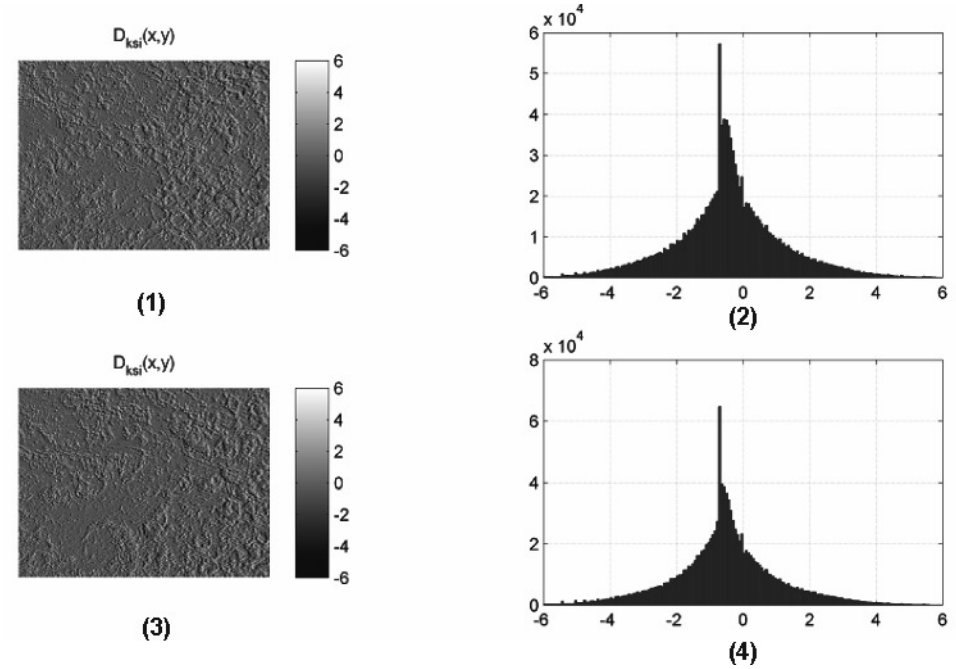

Fig. 2. The maps (fragments (1), (3)) and distribution histograms (fragments (2), (4)) of the magnitude of the fluctuations of the circular dichroism of the optically thick ($\tau = 1{,}19 - 1{,}23; \Lambda = 73\% - 76\%$) histological sections of the kidney are healthy (fragments (1), (2)) and of the diabetic (fragments (3), (4)) rats.

Physically, this can be explained by the following considerations. Necrotic changes caused by the development of diabetes lead to the destruction of the polycrystalline component of the morphological structure of the kidney - the defeat of the amino groups of proteins of the renal glomeruli with the subsequent progression of such changes. Such changes appear in the basal membranes of the blood vessels of the renal glomeruli, cortical, cerebral matter and papilla of the kidney of the rat, which leads to a decrease in the average level of circular birefringence and dichroism, but also the dispersion of their values. Therefore, within the framework of the diffusion tomography method, one should expect a decrease in the fluctuations of the parameters of the circular phase and amplitude anisotropy of the polycrystalline structure of the kidney samples of the diabetic rats.

Quantitative changes of maps D_θ and D_χ diffuse layers of histological sections of the kidney of rats illustrate the statistical moments of the 1st - 4th orders, the mean value and standard deviation of which are within the limits of each control and experimental groups, are given in Table 1.

Table 1 Statistical moments of the 1 st - 4 th orders, which characterize the distribution of magnitude of fluctuations D_θ and D_χ circular birefringence and dichroism of diffuse layers of histological slices of the kidney ($\tau = 1{,}19 - 1{,}23; \Lambda = 73\% - 76\%$) of the healthy and of the diabetic rats

BT	Norm		Diabetes		*Ac*,%	
P_i	D_θ	D_χ	D_θ	D_χ	D_θ	D_χ
P_1	$0{,}14 \pm 0{,}08$	$0{,}05 \pm 0{,}003$	$0{,}12 \pm 0{,}07$	$0{,}04 \pm 0{,}002$	71	69
P_2	$0{,}18 \pm 0{,}011$	$0{,}07 \pm 0{,}004$	$0{,}15 \pm 0{,}08$	$0{,}05 \pm 0{,}003$	75	71
P_3	$0{,}37 \pm 0{,}021$	$1{,}49 \pm 0{,}18$	$0{,}29 \pm 0{,}017$	$1{,}83 \pm 0{,}21$	80	74
P_4	$0{,}26 \pm 0{,}015$	$2{,}12 \pm 0{,}24$	$0{,}35 \pm 0{,}019$	$2{,}56 \pm 0{,}29$	77	73

An analysis of the magnitude of the statistical moments of the 1st to 4th orders that characterize the distribution of the magnitude of the fluctuations of circular birefringence and dichroism (Table 1) revealed a correlation with the physical tendencies analyzed by the changes in the manifestations of the magnitude of fluctuations in the polarization properties of the optically anisotropic diffuse layer of healthy kidneys $P_{i=1;2;3;4}$ compared with transformation of the polycrystalline structure of the optic-thick tissue of the kidney of the diabetic ($P^*_{i=1;2;3;4}$) rats:

$$D_\theta \Leftrightarrow \begin{cases} P_1 \prec P_1^* \Leftrightarrow Ac = 71\%; \\ P_2 \prec P_2^* \Leftrightarrow Ac = 75\%; \\ P_3 \succ P_3^* \Leftrightarrow Ac = 80\%; \\ P_4 \succ P_4^* \Leftrightarrow Ac = 77\%; \end{cases}$$

$$D_\chi \Leftrightarrow \begin{cases} P_1 \prec P_1^* \Leftrightarrow Ac = 69\%; \\ P_2 \prec P_2^* \Leftrightarrow Ac = 71\%; \\ P_3 \succ Z_3^* \Leftrightarrow Ac = 74\%; \\ P_4 \succ P_4^* \Leftrightarrow Ac = 73\%. \end{cases}$$

As can be seen, the level of balanced precision of the diffusion tomography method by mapping the map of elements of the differential matrix of the 2nd order reaches a good level of 75% - 80%. The level of balanced precision of the diffusion tomography using the statistical analysis of the distribution of the magnitude of the circulatory dichroism fluctuations is lower and makes up 69% to 74%. This fact can be associated with a small circular dichroism of protein kidney molecular complexes in the red region of the laser radiation spectrum.

1.4. Maps of fluctuations of circular birefringence and dichroism of parenchymal structures of the liver of the healthy and of the diabetic rats

A series of fig. 3 and rfig. 4 illustrates the results of the method of diffusion tomography - two-dimensional maps $D_j(x, y)$ and histograms $N(D_j)$ of the distribution of the magnitude of the fluctuations of circular birefringence $N(D_j)$ (fig. 3) and dichroism D_χ (fig. 4) of the polycrystalline structure of multiple scattering optic-thick ($\tau = 1{,}19 - 1{,}23; \Lambda = 73\% - 76\%$) histological sections of the liver tissues of healthy (fig. 3, fig. , fragments (1), (2)) and of the diabetic (Fig. 3, Fig. 4, fragments (3), (4)) rats.

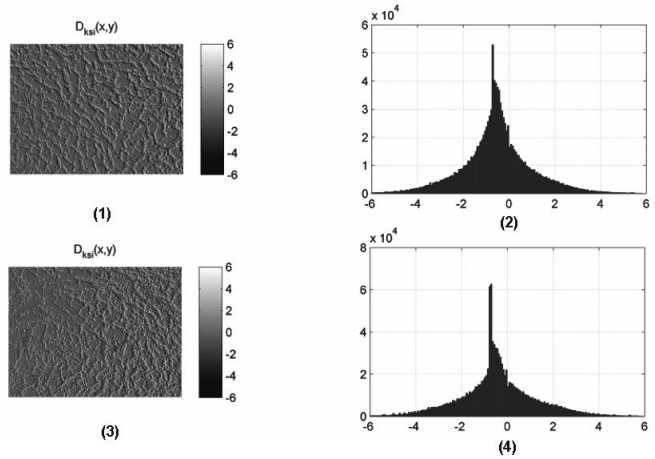

Fig. 3. The maps (fragments (1), (3)) and distribution histograms (fragments (2), (4)) of the magnitudes of the circular birefringence fluctuations of the optically thick ($\tau = 1{,}19 - 1{,}23; \Lambda = 73\% - 76\%$) histological sections of the liver are healthy (fragments (1), (2)) and of the diabetic (fragments (3), (4)) rats.

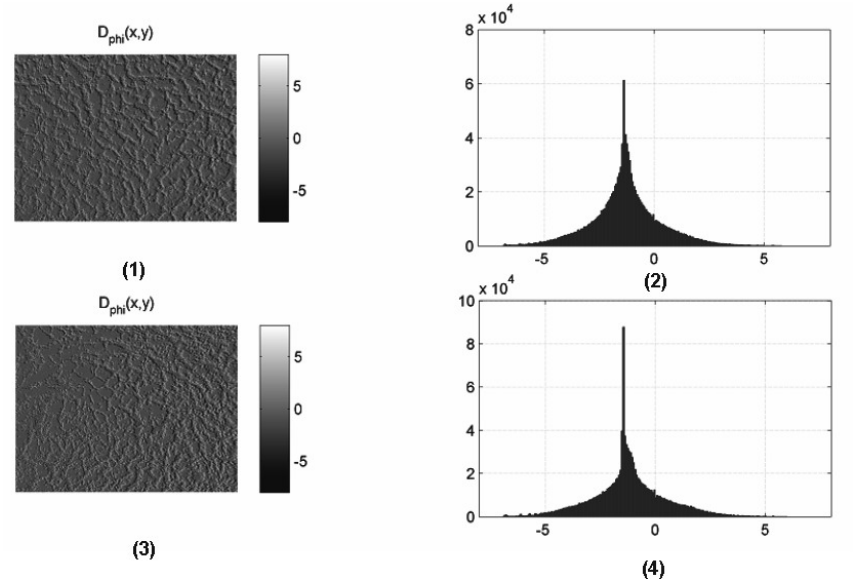

Fig. 4. The maps (fragments (1), (3)) and distribution histograms (fragments (2), (4)) of the magnitude of the fluctuations of the circular dichroism of the optically thick ($\tau = 1{,}19 - 1{,}23; \Lambda = 73\% - 76\%$) histologic sections of the liver are healthy (fragments (1), (2)) and of the diabetic (fragments (3), (4)) rats.

The analysis of the coordinate structure of diffusion tomograms $D_{\theta,\chi}(x,y)$ (fragments (1), (3)) and histograms of distributions $N(D_{\theta,\chi})$ (fragments (2), (4)) of the distribution of the fluctuations of the value of circular birefringence (Fig. 3) and dichroism (Figure 4) are strongly depolarizing ($\tau = 1{,}19 - 1{,}23; \Lambda = 73\% - 76\%$) histological sections of the healthy liver (fragments (1), (2)) and patients with diabetes mellitus (fragments (3), (4)) showed, as for kidney tissue (Figures 3 and 4, fragments (2), (4)) the growth of the mean and the range of spread of the values of such parameters in the maps $D_{\theta,\chi}(x,y)$ of pathologically modified specimens. This is due to the fact that after the introduction of streptotsotocin all the Langerhans islands of the morphological structure of the liver are crushed. This is due to their damage and subsequent resorption of previously necrotized cells. Such a morphological change corresponds to the optical scenario for reducing the level of circular birefringence ($CB \downarrow$) and dichroism ($CD \downarrow$) on the background of minor fluctuations of the linear birefringence (LB) and dichroism (LD), determined by the degree of consistency in shape, size and spatial ordering and coordinate repeatability of molecules within the ensemble of the Langerhans islands. Quantitative changes in the structure of diffusion tomograms D_θ and D_χ scattering layers of the histological sections of the liver of rats illustrate the statistical moments of the 1st to the 4th orders, the mean value and standard deviation of which are within the limits of each control and experimental groups are given in table 2.

Table 2 Statistical moments of the 1st-4th order, which characterize the distribution of magnitude of fluctuations D_θ and D_χ circular birefringence and dichroism of diffuse layers of histological sections of the liver ($\tau = 1{,}19 - 1{,}23; \Lambda = 73\% - 76\%$) of the healthy and of the diabetic rats

	Norm		Diabetes		*Ac*,%	
P_i	D_θ	D_χ	D_θ	D_χ	D_θ	D_χ
P_1	$0{,}08 \pm 0{,}005$	$0{,}05 \pm 0{,}003$	$0{,}06 \pm 0{,}004$	$0{,}04 \pm 0{,}002$	67	61
P_2	$0{,}11 \pm 0{,}006$	$0{,}04 \pm 0{,}002$	$0{,}09 \pm 0{,}005$	$0{,}03 \pm 0{,}002$	66	63
P_3	$1{,}23 \pm 0{,}14$	$1{,}09 \pm 0{,}12$	$1{,}61 \pm 0{,}19$	$1{,}43 \pm 0{,}16$	72	68
P_4	$1{,}76 \pm 0{,}21$	$\pm 0{,}28$	$\pm 0{,}24$	$\pm 0{,}33$	69	6

On the basis of the obtained data (a set of magnitudes of statistical moments of the 1st - 4th orders that characterize the distribution of the magnitudes of the fluctuations of circular birefringence and dichroism - Table 2), correlation was established with the physical tendencies of the manifestations of magnitude fluctuations in the polarization properties of the optically anisotropic parenchymal layer of the liver of healthy ($P_{i=1;2;3;4}$) in comparison with the transformation of the polycrystalline structure of the optic-thick liver tissue of the diabetic ($P^{*}_{i=1;2;3;4}$) rats:

$$D_{\theta} \Leftrightarrow \begin{cases} P_1 \prec P_1^{*} \Leftrightarrow Ac = 67\%; \\ P_2 \prec P_2^{*} \Leftrightarrow Ac = 66\%; \\ P_3 \succ P_3^{*} \Leftrightarrow Ac = 77\%; \\ P_4 \succ P_4^{*} \Leftrightarrow Ac = 73\%; \end{cases}$$

$$D_{\chi} \Leftrightarrow \begin{cases} P_1 \prec P_1^{*} \Leftrightarrow Ac = 61\%; \\ P_2 \prec P_2^{*} \Leftrightarrow Ac = 63\%; \\ P_3 \succ P_3^{*} \Leftrightarrow Ac = 68\%; \\ P_4 \succ P_4^{*} \Leftrightarrow Ac = 65\%. \end{cases}$$

As can be seen, the level of balanced accuracy of the diffusion tomography method by mapping the map of elements of the differential matrix of the 2nd order reaches a satisfactory level of 73% -77%. The level of balanced precision of the diffusion tomography using the statistical analysis of the distribution of the magnitude of the fluctuations of the circular dichroism is less and is 65% -68%.

2. Clinical application of the diffusion tomography method

2.1. Differential diagnosis of tumors of the uterus wall

Two groups of histological sections of the tumors of the uterine wall were investigated:

- benign tumor (adenoma) - group 1 (17 samples);
- malignant tumor (carcinoma) - group 2 (17 samples).

Table 3 presents the values of the balanced accuracy of the diffuse tomography method.

Table 3 Balanced accuracy of differential diagnostics of tumors of the uterine wall by diffuse tomography

P_i	D_{θ},	D_{χ}
P_1	71%	67%
P_2	73%	71%
P_3	81%	76%
P_4	85%	80%

A good level of balanced accuracy (85%) of differential diagnostics of the tumors of the uterus wall has been achieved, using the diffuse tomography of the distribution of the magnitude of the fluctuations of the linear birefringence of the polycrystalline component of the histological sections.

2.2. Differentiation of the degree of blood loss in the liver

Two groups of histological sections of the liver of the deceased were studied:

- blood loss 1 liter - group 1 (12 samples);
- stage of blood loss 2 liters - Group 1 (12 samples).Table 4 presents the values of the balanced accuracy of the diffuse tomography method.

Table 4 Balanced accuracy of differential diagnosis of the degree of blood loss of the liver of the deceased by diffuse tomography

P_i	D_θ,	D_χ
P_1	78%	72%
P_2	83%	73%
P_3	85%	78%
P_4	89%	86%

Achieved a very good level of balanced accuracy (89%) of differential diagnosis of the degree of blood loss of the liver of the deceased by the method of diffuse tomography of the distribution of the magnitude of the fluctuations of the linear birefringence of the polycrystalline component of the histological sections.

Conclusions

1. A structural-logical scheme was developed and experimentally tested the technique of diffusion tomography with the definition of depolarization maps as well as distribution of the magnitude of the set of elements of the differential matrix of the 2nd order, which are the basis for the polarization reproduction of the fluctuations of the parameters of phase and amplitude anisotropy of the polycrystalline structure of highly depolarizing layers of biological tissues different morphological structure and pathological condition.
2. The objective criteria for the diffusion tomographic differentiation of the distribution of the magnitude of the fluctuations of the parameters of the circular phase (asymmetry and excess $P_{3;4}(D_\theta)$ - differences vary from 1.32 to 1.37 times) and the amplitude ($P_{3;4}(D_\chi)$- differences make up 1.29 - 1.34 times) anisotropy of polycrystalline structures histological sections of the internal organs of the healthy and of the diabetic rats . On this basis, a satisfactory level of balanced accuracy of the differential diagnosis of changes in the polycrystalline structure due to this pathology $Ac(P_{3;4}(D_\theta(x,y)); D_\chi(x,y))) \succ 80\%$ has been achieved.
3. Implemented with good balanced accuracy (85%) of the differentiation of the magnitude of the fluctuations of the linear birefringence of diffuse samples of benign and malignant tumors of the uterus wall.
4. Objective criteria for differentiation of the degree of blood loss of the liver of the deceased by diffuse tomography with a very good (89%) balanced accuracy were found.

References

[1] De Martino, Ed., "A polarization-based optical techniques applied to biology and medicine," in Proc. European Workshop, Ecole Polytechnique, Massy, France (2009).

[2] N. Ghosh and I. A. Vitkin, "Tissue polarimetry: concepts, challenges, applications and outlook," J. Biomed. Opt. 16, 110801 (2011).

[3] S. L. Jacques, "Polarized light imaging of biological tissues" in Handbook of Biomedical Optics, D. Boas, C. Pitris, and N. Ramanujam, Eds., pp. 649–669, CRC Press, Boca Raton, London, New York (2011).

[4] N. Ghosh, M. F. G. Wood, and I. A. Vitkin, "Polarized light assessment of complex turbid media such as biological tissues via Mueller matrix decomposition," in Handbook of Photonics for Biomedical Science, V. V. Tuchin, Ed., pp. 253–282, CRC Press, Taylor & Francis Group, London (2010).

[5] D. Layden, N. Ghosh, and A. Vitkin, "Quantitative polarimetry for tissue characterization and diagnosis," in Advanced Biophotonics: Tissue Optical Sectioning, R. K. Wang and V. V. Tuchin, Eds., pp. 73–108, CRC Press, Taylor & Francis Group, Boca Raton, London, New York (2013).
[6] A. Vitkin, N. Ghosh, and A. de Martino, "Tissue polarimetry" in Photonics: Scientific Foundations, Technology and Applications, D. L. Andrews, Ed., Vol. IV, pp. 239–321, John Wiley & Sons, Inc., Hoboken, New Jersey (2015).
[7] M. I. Mishchenko, L. D. Travis, and A. A. Lacis, Scattering, Absorption, and Emission of Light by Small Particles, Cambridge University Press, Cambridge (2002).
[8] M. K. Swami, H. S. Patel, and P. K. Gupta, "Conversion of 3 × 3 Mueller matrix to 4 × 4 Mueller matrix for non-depolarizing samples," Opt. Commun. 286(1), 18–22 (2013).
[9] V. F. Izotova et al., "Investigation of Mueller matrices of anisotropic nonhomogeneous layers in application to optical model of cornea," Appl. Opt. 36(1), 164–169 (1997).
[10] V. V. Tuchin, "Tissue optics and photonics: biological tissue structures [review]," J. Biomed. Photonics Eng. 1(1), 3–21 (2015).
[11] V. V. Tuchin, "Tissue optics and photonics: light-tissue interaction [review]," J. Biomed. Photonics Eng. 1(2), 98–134 (2015).
[12] S. Manhas et al., "Mueller matrix approach for determination of optical rotation in chiral turbid media in backscattering geometry," Opt. Express 14(1), 190–202 (2006).
[13] Y. Deng et al., "Characterization of backscattering Mueller matrix patterns of highly scattering media with triple scattering assumption," Opt. Express 15(15), 9672–9680 (2007).
[14] Alexander G. Ushenko and Vasilii P. Pishak, "Laser Polarimetry of Biological Tissue: Principles and Applications", in Handbook of Coherent-Domain Optical Methods: Biomedical Diagnostics, Environmental and Material Science, vol. I, Valery V. Tuchin, Ed. Boston: Kluwer Academic Publishers, 2004, pp. 93-138.
[15] O. V. Angelsky, A. G. Ushenko, Yu. A. Ushenko, V. P. Pishak, A. P. Peresunko, "Statistical, Correlation and Topological Approaches in Diagnostics of the Structure and Physiological State of Birefringent Biological Tissues" in Handbook of Photonics for Biomedical Science, pp. 283-322 ed. by Valery V. Tuchin, CRC PressTaylor&Francis group: Boca Raton, London, New York (2010).
[16] Y. A. Ushenko, T. M. Boychuk, V. T. Bachynsky, O. P. Mincer, "Diagnostics of Structure and Physiological State of Birefringent Biological Tissues: Statistical, Correlation and Topological Approaches" in Handbook of Coherent-Domain Optical Methods, Springer Science+Business Media, p. 107, New York (2013).
[17] S. Y. Lu and R. A. Chipman, "Interpretation of Mueller matrices based on polar decomposition," J. Opt. Soc. Am. A 13(5), 1106– 1113 (1996).
[18] Y. Guo et al., "A study on forward scattering Mueller matrix decomposition in anisotropic medium," Opt. Express 21(15), 18361–18370 (2013).
[19] B. Deboo, J. Sasian, and R. A. Chipman, "Degree of polarization surfaces and maps for analysis of depolarization," Opt. Express 12(20), 4941–4958 (2004).
[20] I. C. Buscemi and S. Guyot, "Near real-time polarimetric imaging system," J. Biomed. Opt. 18(11), 116002 (2013).
[21] S. Manhas et al., "Demonstration of full 4 × 4 Mueller polarimetry through an optical fiber for endoscopic applications," Opt. Express 23(3), 3047–3054 (2015).
[22] A. Pierangelo et al., "Multispectral Mueller polarimetric imaging detecting residual cancer and cancer regression after neoadjuvant treatment for colorectal carcinomas," J. Biomed. Opt. 18(4), 046014 (2013).
[23] L. V. Wang and H.-I. Wu, Biomedical Optics: Principles and Imaging, Wiley-Interscience, Hoboken, New Jersey (2007).
[24] D. Boas, C. Pitris, and N. Ramanujam, Eds., Handbook of Biomedical Optics, CRC Press, Boca Raton, London, New York (2011).
[25] T. Vo-Dinh, Ed., Biomedical Photonics Handbook, 2nd ed., CRC Press, Boca Raton (2014).
[26] V. V. Tuchin, Tissue Optics: Light Scattering Methods and Instruments for Medical Diagnostics, 3rd ed., Vol. PM 254, SPIE Press, Bellingham, Washington (2015).
[27] Lu S. Interpretation of Mueller matrices based on polar decomposition / S. Lu, R. A. Chipman // J. Opt. Soc. Am. A, Vol.13, 1106–1113, 1996.
[28] N. Ortega-Quijano, J.L. Arce-Diego, "Mueller matrix differential decomposition," Opt. Letters 36, 1942-1944 (2011).
[29] N. Ortega-Quijano, J.L. Arce-Diego, "Depolarizing differential Mueller matrices," Opt. Letters 36, 2429-2431 (2011).
[30] R. Ossikovski, V. Devlaminck, " General criterion for the physical realizability of the differential Mueller matrix," Opt. Lett. 39, 1216-1219 (2014).
[31] V. Devlaminck and R. Ossikovski, "Uniqueness of the differential Mueller matrix of uniform homogeneous media," Opt. Lett. 39, 3149-3152 (2014).
[32] V. Devlaminck, "Physical model of differential Mueller matrix for depolarizing uniform media," J. Opt. Soc. Am. 30, 2196-2204 (2013) .
[33] R. Ossikovski, O. Arteaga, "Statistical meaning of the differential Mueller matrix of depolarizing homogeneous media," Opt. Lett. 39, 4470-4473 (2014) .
[34] Angelsky, O.V., Maksimyak, P.P., Ryukhtin, V.V., Hanson, S.G., "New feasibilities for characterizing rough surfaces by optical-correlation techniques," Applied Optics, 40 (31), 5693-5707 (2001).
[35] Angelsky, O.V., Maksimyak, P.P., "Optical diagnostics of random phase objects," Applied Optics, 29 (19), 2894-2898 (1990).

[36] Angelsky, O. V., Bekshaev, A. Ya., Maksimyak, P. P., Maksimyak, A. P., Hanson, S. G., and Kontush, S. M., "Controllable generation and manipulation of micro-bubbles in water with absorptive colloid particles by CW laser radiation," Opt. Express 25, 5232-5243 (2017).
[37] O.V. Angelsky, S.G. Hanson, P.P. Maksimyak, A.P. Maksimyak, C.Yu. Zenkova, P.V. Polyanskii, and D.I. Ivanskyi, "Influence of evanescent wave on birefringent microplates," Opt. Express 25, 2299-2311 (2017).